THE ASTROPHYSICAL JOURNAL, 513:L127–L130, 1999 March 10

NICMOS IMAGING OF THE HR 4796A CIRCUMSTELLAR DISK

GLENN SCHNEIDER,[1] BRADFORD A. SMITH,[2] E. E. BECKLIN,[3] DAVID W. KOERNER,[4] ROLAND MEIER,[2] DEAN C. HINES,[1] PATRICK J. LOWRANCE,[3] RICHARD J. TERRILE,[5] RODGER I. THOMPSON,[1] AND MARCIA RIEKE[1]

Received 1998 November 24; accepted 1999 January 13; published 1999 February 9

ABSTRACT

We report the first near-infrared (NIR) imaging of a circumstellar annular disk around the young (~8 Myr), Vega-like star HR 4796A. NICMOS coronagraph observations at 1.1 and 1.6 μm reveal a ringlike symmetrical structure that peaks in reflected intensity 1.″05 ± 0.″02 (~70 AU) from the central A0 V star. The ring geometry, with an inclination of 73.°1 ± 1.°2 and a major axis position angle of 26.°8 ± 0.°6, is in good agreement with recent 12.5 and 20.8 μm observations of a truncated disk. The ring is resolved with a characteristic width of less than 0.″26 (17 AU) and appears abruptly truncated at both the inner and outer edges. The region of the disk-plane inward of ~60 AU appears to be relatively free of scattering material. The integrated flux density of the part of the disk that is visible (greater than 0.″65 from the star) is found to be 7.6 ± 0.5 and 7.4 ± 1.2 mJy at 1.1 and 1.6 μm, respectively. Correcting for the unseen area of the ring yields total flux densities of 12.8 ± 1.0 and 12.5 ± 2.0 mJy, respectively (Vega magnitudes equal to 12.92 ± 0.08 and 12.35 ± 0.18). The NIR luminosity ratio is evaluated from these results and ground-based photometry of the star. At these wavelengths, $L_{\rm disk}(\lambda)/L_*(\lambda)$ is equal to $1.4 \pm 0.2 \times 10^{-3}$ and $2.4 \pm 0.5 \times 10^{-3}$, giving reasonable agreement between the stellar flux scattered in the NIR and that which is absorbed in the visible and reradiated in the thermal infrared. The somewhat red reflectance of the disk at these wavelengths implies a mean particle size in excess of several microns, which is larger than typical interstellar grains. The confinement of material to a relatively narrow annular zone implies dynamical constraints on the disk particles by one or more as yet unseen bodies.

Subject headings: circumstellar matter — infrared: stars — planetary systems — stars: individual (HR 4796A)

1. INTRODUCTION

HR 4796A ($V = 5.78$ and $d = 67 \pm 3.5$ pc, as determined by *Hipparcos*) is a young A0 V star (Houk 1982) with an estimated age of 8 ± 3 Myr (Stauffer et al. 1995; Jayawardhana et al. 1998). It has been the object of much scrutiny since Jura (1991) inferred the presence of an unusually large amount of circumstellar dust, based on an analysis of *IRAS* data. Jura's initial estimate of the dust opacity, $\tau_{\rm dust} = L_{\rm dust}/L_* = 5 \times 10^{-3}$, exceeds by a factor of 2 that of β Pictoris, which was then the only main-sequence star for which a circumstellar disk had been optically imaged (Smith & Terrile 1984). Jura et al. (1995) noted that their earlier estimated dust temperature (110 K) indicated a lack of disk material within 40 AU of HR 4796A. They required a minimum grain size of ~3 μm for the particles to remain gravitationally bound and suggested that this material is located between 40 and 200 AU from the star. They further suggested that grains of this size must have coalesced from smaller particles, with a much higher growth rate into larger particles taking place within 40 AU of the star. Their 2 μm speckle data and optical spectra ruled out any close stellar "sweeper" companions with $M_* > 0.125\ M_\odot$ as close as 11 AU that could be responsible for such a central clearing (Artymowicz & Lubow 1994), but left open the possibility of lower mass companions.

Recently, a circumstellar disk around HR 4796A was imaged at 12.5 and 20.8 μm by Koerner et al. (1998) and observed independently at lower resolution by Jayawardhana et al. (1998) at 18.2 μm. An inner depleted region was apparent in the high-resolution 20.8 μm image, and this was reproduced by a model of the emission from a disk with inclination $i = 72°$ (+6°, −9°), position angle 28° ± 6°, and inner radius $R_{\rm in} \sim 55$ AU. Additional constraints from long-wavelength flux densities yielded an outer radius of $R_{\rm out} \sim 80$ AU. In contrast, the excess 12.5 μm emission appeared centered on the star and, together with small residuals from the fit at 20.8 μm, indicated the presence of a tenuous warm dust component confined to within a few AU of the star. These results were interpreted by Koerner et al. (1998) to indicate the presence of an inner compact "zodiacal dust" component surrounded by a more prominent dust ring at a radial distance corresponding to the Kuiper Belt.

Ground-based attempts to image the HR 4796A disk in reflected light (e.g., Mouillet et al. 1997) have thus far failed. However, Near-Infrared Camera and Multi-Object Spectrometer (NICMOS) 1.1 and 1.6 μm images of a ringlike circumstellar annular disk about HR 4796A now provide, for the first time, spatially resolved photometric properties of the disk, and more precisely define its morphology. A first-look analysis of the data is reported here. Detailed modeling of the geometric and photometric properties of the disk will be discussed in a later paper.

2. NICMOS CORONAGRAPHIC OBSERVATIONS

NICMOS Camera 2 coronagraphic observations of HR 4796A were obtained at two epochs: 1998 March 15 and August 16. The initial observations, in which both the northeast and southwest ansae of the annulus were detected, were obtained in H band (F160W filter; $\lambda_{\rm central} = 1.594$ μm, $\Delta\lambda = 0.403$ μm). The second-epoch follow-up observations employed both the F160W and F110W ($\lambda_{\rm central} = 1.0998$ μm,

[1] Steward Observatory, University of Arizona, 933 North Cherry Avenue, Tucson, AZ 85721; gschneider@as.arizona.edu, dhines@as.arizona.edu, rthompson@as.arizona.edu, marcia@as.arizona.edu.

[2] Institute for Astronomy, University of Hawaii, Honolulu, HI 96720; brad@mahina.ifa.hawaii.edu, meier@hale.ifa.hawaii.edu.

[3] Department of Physics and Astronomy, University of California Los Angeles, Los Angeles, CA 90095; becklin@sofia.astro.ucla.edu, lowrance@astro.ucla.edu.

[4] University of Pennsylvania, 4N14 DRL, 209 South 33d Street, Philadelphia, PA 19104; davidk@upenn5.hep.upenn.edu.

[5] Jet Propulsion Laboratory, MS 183-503, Pasadena, CA 91109; Richard.J.Terrile@jpl.nasa.gov.

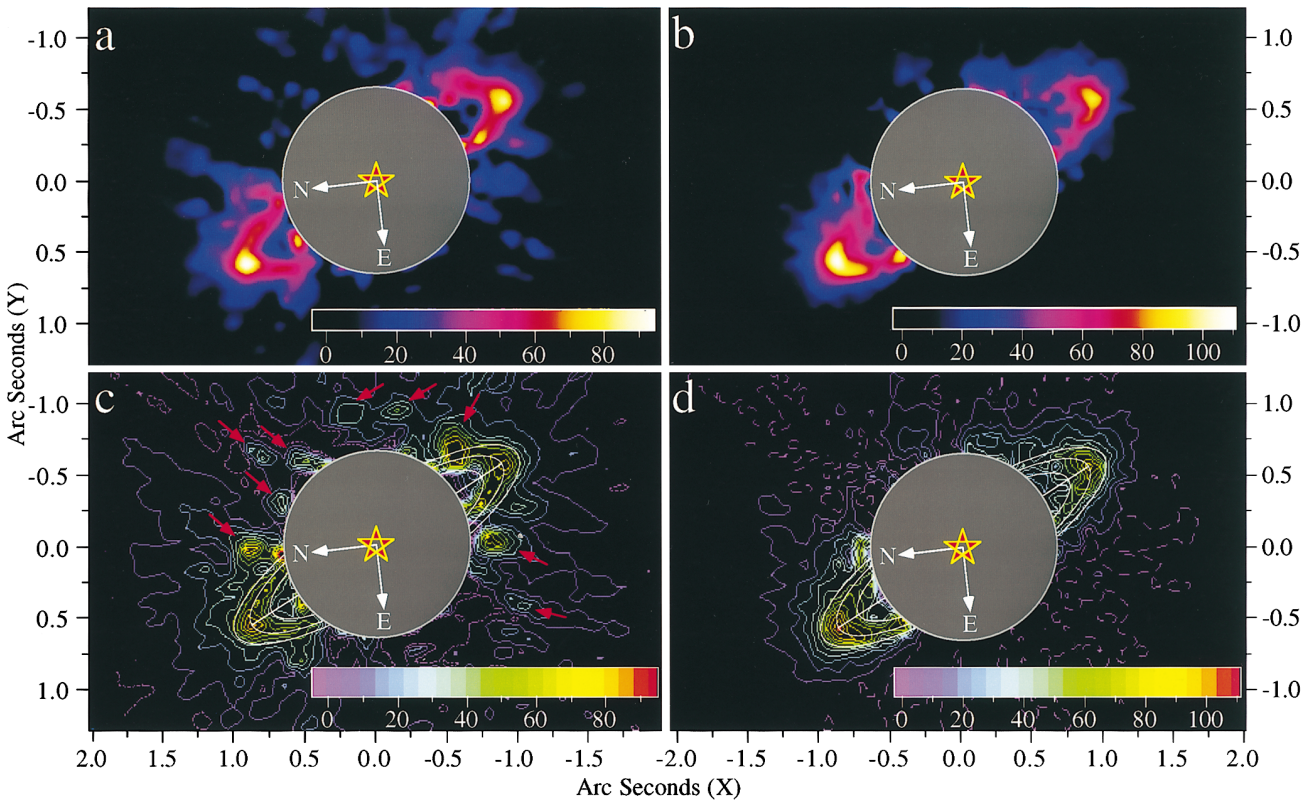

FIG. 1.—Images and 10 μJy isophotal maps of the HR 4796A circumstellar ring. (*a*, *c*) 1.6 μm (F160W), 1998 March 15. (*b*, *d*) 1.1 μm (F110W), 1998 August 16. The unusable area circumscribing the coronagraphic hole is indicated (*gray circles*). A few artifacts in the 1.6 μm image remain at larger radii arising from an imperfectly matched stellar PSF and are identified in panel *c* (*red arrows*). These were removed in panel *a* based on comparison of this PSF subtraction with the second-epoch F160W images and a priori knowledge of the NICMOS coronagraphic pupil function. The coronagraph and detector were rotated 168°.8 between observational epochs, aiding in the identification (and rejection) of optical artifacts. Color bars give flux densities in μJy per Camera 2 pixel (0″.0762 × 0″.0755, both $\pm$0″.0002).

$\Delta\lambda = 0.592$ μm) filters. Although the geometrical radius of the coronagraph hole is 0″.3, instrumental scatter, diffraction, and point-spread function (PSF) misregistration extended the radius of nonusable data to ~0″.65. To further facilitate discrimination of PSF artifacts (which are more prevalent at 1.6 μm) from intrinsic morphological features of the circumstellar disk, the rotational orientations of the field at each epoch differed by 168°.8.

By obtaining coronagraphic images at different field orientations (by rotating the spacecraft about the target axis), it is possible to differentiate unocculted circumstellar objects and features from artifacts caused by instrumental scattering and the complex *Hubble Space Telescope*+NICMOS pupil function. Optical/instrumental artifacts corotate with the detector, while objects/features in the target image do not. The detection of faint pointlike objects, or low surface brightness extended features of angular azimuthal extent smaller than their position displacements due to field rotation, is made possible by subtracting the second roll orientation image from the first, thereby nulling the unocculted wings of the occulted bright target PSF. This works extremely well to the level of the residual photon noise if the target is repositioned in the coronagraph hole with high precision following a spacecraft roll (Schneider et al. 1998). Individual sets of images were obtained within 25 minute intervals to minimize PSF variations that arise from "breathing" of the *Hubble Space Telescope* (*HST*) optical telescope assembly (Bely 1993). To eliminate image artifacts known as "the bars" (see NICMOS Image Anomalies[6]), Cameras 1 and 3 were run simultaneously (but blanked off in ACCUM mode) during all of the Camera 2 observations.

The 1998 March 15 (first epoch) observations were carried out using an observing strategy described by Lowrance et al. (1998) and adopted for the search/detection phases of the NICMOS Environments of Nearby Stars (EONS) observing programs (Schneider 1998). Imaging sequences were executed with a total integration time of 672 s at each of two image orientation angles differing by 29°.9. However, data from the second orientation were significantly degraded due to a guide star acquisition failure and could not be used. An available reference PSF from unrelated observations of CoD $-33°7795$ (Lowrance et al. 1999) was subtracted from the data. The difference image indicated the presence of excess flux, spatially coincident with the locations of the brightest parts of the 20.8 μm disk found by Koerner et al. (1998). Based on this initial 1.6 μm detection, follow-up observations were planned for 1998 August 16 after HR 4796A came out of *HST* solar avoidance. Later, a ringlike annular disk was clearly seen in this first-epoch data after subtracting a better matched PSF from another star (51 Oph; see Fig. 1*a*).

Observations at 1.1 μm were added at the second epoch to obtain color information on the disk. Instrumental scatter at

[6] Available at http://www.stsci.edu/ftp/instrument_news/NICMOS/nicmos_anomalies.html#BRS.

small radial distances from the edge of the coronagraph hole is reduced significantly at shorter wavelengths, due to the smaller spatial scale of the higher resolution PSF. These F110W coronagraphic images were obtained at two spacecraft roll orientations, used here as a "roll dither" to replace bad pixels rather than for difference-imaging source detection. Because of the Sun-angle and available guide-star constraints, a differential roll of only 9° was possible. At 1″ (where the 1.6 μm excess flux peaked in the initial detection image), a 9° roll results in a field rotation of 0.″158, slightly more than 2 pixels. This exceeds the FWHM of the PSF at 1.1 μm by ~32%. Thus, beyond the 0.″65 inner usable radius, roll-paired images may be effectively resampled around bad pixels. The total integration time of the F110W data was 1952 s. Four F160W images, with a total integration time of 1024 s, were obtained at a single field orientation that differed from that of the March 15 observations.

At the second roll position, the spacecraft was slewed to a nearby bright star of similar spectral type (B8 V), HR 4748 ($H = 5.44$), to produce a contemporaneous F110W coronagraphic reference PSF in the same orbit. This star exhibited no evidence of multiplicity in previous ground- and space-based observations. A total integration time of 576 s was used to achieve a signal-to-noise ratio (S/N) comparable to that obtained for HR 4796A.

3. DATA CALIBRATION AND REDUCTION

The raw MULTIACCUM image data were calibrated with an analog to STScI's CALNICA pipeline software, with three differences in processing: (1) Before the standard linearity corrections, flux estimates were made for pixels that were driven into nonlinearity in the first or second read of the detector following the initial reset. (2) Cosmic-ray hits were detected (and subsequently compensated for) with a sigma-clipped cosmic-ray rejection procedure. (3) Corrections were made for residual DC pedestals and quadrant-dependent DC offsets in the detector. These steps were taken before flat-fielding the derived count-rate image. Calibration dark reference files made from on-orbit darks by the NICMOS Instrument Definition Team (IDT) were used. Standard Camera 2 bad pixel maps were updated for changes in underresponsive pixels from contemporaneous, background-subtracted, F160W flat fields obtained as part of the target acquisition (TA) process. In the case of the F160W imaging, the reference flat fields themselves were augmented near the edge of the coronagraph hole with the TA flats to better compensate for short-term drifts of the hole position. While TA flats are inherently of lower S/N (~100) than standard calibration flats (S/N ~ 1200), this is more than sufficient to remove those artificial edge gradients that are otherwise introduced by the application of uncorrected flat fields. Because translational dithering is generally not feasible in coronagraphic observations, bad pixels in the flux-calibrated frames were replaced by two-dimensional Gaussian-weighted interpolation. A weighting radius of 3 pixels was used for the F110W data and 5 pixels for the F160W data. After bad-pixel replacement, the fluxes derived from the calibrated MULTIACCUMs were averaged with equal weighting. This process was applied to the HR 4796A (F110W and F160W), HR 4748 (F110W), and 51 Oph (F160W) MULTIACCUM images.

The HR 4748 and 51 Oph calibrated reference PSFs were subtracted from the HR 4976A F110W and first-epoch F160W calibrated images using the IDP3 program developed by the NICMOS IDT (Lytle et al. 1999). The reference PSFs were rescaled in flux to match the stellar component of the HR 4796A images. Reregistration was accomplished through bicubic convolution interpolation (Park & Schowengerdt 1983). The residual energy along the three-component diffraction spikes was measured (at radii where the circumstellar source flux is not contributing significantly) and effectively removed (Fig. 1*b*) in the F110W PSF-subtracted image.

4. GEOMETRY, MORPHOLOGY, AND PHOTOMETRY

4.1. *Geometry*

Implicit in this analysis is the assumption that the observed circumstellar ring structure is circular. The orientation, inclination, and mean radius of the circumstellar ring were found, independently, from the first- and second-epoch F160W (single orientation) and second-epoch F110W (combined two-orientation) images by least-squares ellipse fitting of the "midring" and the inner and outer half-peak intensity contours. The solutions from each data set were constrained such that the resulting fits to the isophotes were required to be concentric. In all three cases, the parametric solutions overlapped within their errors. The solution from the F110W observations, which have the highest statistical significance, has been adopted. These observations are of higher S/N and are less biased by the influence of residual PSF artifacts than those of the F160W observations. The solution yields a position angle of 26.°8 ± 0.°6, an inclination of 73.°1 ± 1.°2, and a semimajor axis of 1.″05 ± 0.″02 for the projected ring ellipse. Assuming a distance to HR 4796 of ~67 pc, this corresponds to a physical radius of 70.4 ± 1.4 AU, in excellent agreement with Koerner et al. (1998) [P.A. = 28° ± 6°, $i = 72°$ $(+6°, -9°)$, $r = 67.5 \pm 12.5$ AU]. In the F110W data, no statistically significant deviations from ellipticity were found. The ellipse fits are superposed on 1.6 and 1.1 μm isophotal maps of the HR 4796A disk in Figures 1*c* and 1*d*. It is important to emphasize here that these solutions are based solely on observed isophotes and do not, as yet, consider the scattering properties of the disk material.

4.2. *Morphology*

The ring appears to be abruptly bounded both interior and exterior to the midring ($r \sim 70$ AU) in both the 1.1 and 1.6 μm images. At 1.1 μm, the FWHM of the mean radial component of the peak intensities of the ansae is less than 0.″29 (~20 AU). The measured profile is broadened by the coronagraphic PSF, which itself has a FWHM of 0.″12 (8 AU at the distance of HR 4796). Quadratic subtraction of the PSF yields an actual photometric full width of the disk annulus equal to or less than 0.″26 (17 AU). No significant level of scattered radiation is seen inward from ~60 to ~45 AU where the residual photon noise from the bright central star dominates the measurements.

4.3. *Photometry*

Figures 1*c* and 1*d* show the measured flux isophotes of the HR 4796A disk at both 1.1 and 1.6 μm. Photometric calibration constants of 2.195×10^{-6} and 2.207×10^{-6} Jy ADU^{-1} s^{-1} (M. Rieke, unpublished data) were used to convert from instrumental count rates to physical units for the F110W and F160W filters, respectively.

The total reflected energy outside a radius of 0.″65 was es-

timated by summing the flux within a rectangular region of ~3.″1 × 0.″9 (corresponding to the axial ratio of the disk, but oversized by 50%) oriented along the disk major axis. In doing so, the residual background from four nearby regions adjacent to this area was subtracted and the photometric error, as determined from the background variations, was estimated. In the F160W image, spurious PSF artifacts were removed by treating them as regions of "missing data" and then interpolating bicubically over the small areas. The total flux measured was 7.6 ± 0.5 mJy at 1.1 μm and 7.4 ± 1.2 mJy at 1.6 μm. The area of ring that is contained within the inner 0.″65 radius region, and is thus not measurable, is ~40.8% of the total area. Applying an areal correction (and assuming uniform surface brightness), the total flux is found to be 12.8 ± 1.0 mJy at 1.1 μm and 12.5 ± 2.0 mJy at 1.6 μm. Zero points for the photometric conversions, also from M. Rieke (unpublished data), are 1909 and 1087 Jy for an $H = 0.0$ source for the F110W and F160W filters, respectively. These give integrated Vega magnitudes for the ring of 12.92 ± 0.08 (F110W) and 12.35 (−0.19, +0.16) (F160W). Using ground-based multicolor photometry of HR 4796A (Jura et al. 1993; $I = 5.81$, $J = 5.80$, $H = 5.80$, all ±0.10), the near-infrared (NIR) optical depth is $\tau_{\rm NIR} \sim L_{\rm disk}(\lambda)/L_*(\lambda) = 1.4 \pm 0.2 \times 10^{-3}$ and $2.4 \pm 0.5 \times 10^{-3}$, respectively. Thus, there is first-order agreement between the stellar flux scattered by the circumstellar dust in the NIR and that which is absorbed in the visible and reradiated by the dust in the thermal infrared ($L_{\rm disk}/L_* = 5 \times 10^{-3}$). Within the photometric errors, the ring appears to be somewhat red in reflection. This suggests that the mean disk-particle size must be larger than several microns, indicating debris origin rather than trapped interstellar dust.

5. SUMMARY AND CONCLUSIONS

NICMOS 1.1 μm (F110W) and 1.6 μm (F160W) coronagraphic observations have for the first time imaged the HR 4796A circumstellar disk in reflected light, revealing a narrow, ringlike structure. These images provide spatially resolved geometric and photometric properties of the disk using the high angular resolution offered by *HST*. The ring, with a mean radius of approximately 70 AU, appears sharply bounded and narrow (less than 17 AU). The NICMOS observations effectively probe the circumstellar environment inward to a radius of ~45 AU from the central star and confirm the depletion of disk material inferred by earlier observers (e.g., Jura et al. 1993) and, more recently, by direct observations at 20.8 μm (Koerner et al. 1998). The observed flux ratio is $L_{\rm disk}(\lambda)/L_*(\lambda) = 1.4 \pm 0.2 \times 10^{-3}$ at 1.1 μm and $2.4 \pm 0.5 \times 10^{-3}$ at 1.6 μm, indicating somewhat red reflection. This implies a mean particle size that is large compared to these wavelengths. Assuming $\tau_{\rm dust} \sim L_{\rm disk}(\lambda)/L_*(\lambda)$, there is reasonable agreement between the scattered stellar flux in the NIR and that which is absorbed in the visible and reradiated in the thermal infrared. The stable containment of ring particles and the abrupt inner and outer truncation of the ring around this relatively young star imply dynamical constraints (Goldreich & Tremaine 1979) imposed by one or more related, but as yet unseen, bodies. How such bodies, presumably planets, could have formed so quickly at such large distances from the star presents an interesting challenge to those who model planet formation.

The NICMOS EONS group wishes to acknowledge the contributions made to this program by the other members of the NICMOS IDT. We thank our program coordinator, Douglas Van Orsow, and contact scientist, Alfred Schutz, at STScI for the assistance in implementing and scheduling our *HST*/EONS observations. This work is supported by NASA grant NAG5-3042. This Letter is based on observations with the NASA/ESA *Hubble Space Telescope*, obtained at the Space Telescope Science Institute, which is operated by the Association of Universities for Research in Astronomy, Inc. under NASA contract NAS5-26555.

REFERENCES

Artymowicz, P., & Lubow, S. H. 1994, ApJ, 337, 494
Bely, P. 1993, STScI Report SESD-93-16 (Baltimore: Space Telescope Science Institute)
Goldreich, P., & Tremaine, S. 1979, Nature, 277, 97
Houk, N. 1992, Michigan Spectral Catalog, Vol. 3 (Ann Arbor: Univ. of Michigan Press)
Jayawardhana, R., Fisher, S., Hartmann, L., Telesco, C., Pina, R., & Fazio, G. 1998, ApJ, 503, 79
Jura, M. 1991, ApJ, 383, L79
Jura, M., Ghez, A. M., White, R. J., McCarthy, D. W., Smith, R. C., & Martin, P. G. 1995, ApJ, 445, 451
Jura, M., Zuckerman, B., Becklin, E. E., & Smith, R. C. 1993, ApJ, 418, L37
Koerner, D. W., Ressler, M. E., Werner, M. W., & Backman, D. E. 1998, ApJ, 503, L83
Lowrance, P. J., et al. 1998, in NICMOS and the VLT: A New Era of High-Resolution Near-Infrared Imaging and Spectroscopy, ed. W. Freudling & R. Hook (ESO Conf. Workshop Proc. 55; Garching, ESO), 96
Lowrance, P. J., et al. 1999, ApJ, 512, L69
Lytle, D., Stobie, E., Ferro, A., & Barg, I. 1999, ASP Conf. Ser., Astronomical Data Analysis Software and Systems 8, ed. D. Mehringer, R. Plante, & D. Roberts (San Francisco: ASP), in press
Mouillet, D., Lagrange, A.-M., Beuzit, J.-L., & Renaud, N. 1997, A&A, 324, 1083
Park, S., & Schowengerdt, R. 1983, Comput. Vision, Graphics, Image Processing, 23, 256
Schneider, G. 1998, NICMOS and the VLT: A New Era of High-Resolution Near-Infrared Imaging and Spectroscopy, ed. W. Freudling & R. Hook (ESO Conf. Workshop Proc. 55; Garching: ESO), 88
Schneider, G., Thompson, R. I., Smith, B. A., & Terrile, R. J. 1998, Proc. SPIE, 3356, 222
Smith, B. A., & Terrile, R. J. 1984, Science, 226, 1421
Stauffer, J. R., Hartman, L. W., & Navascues Y Barrado, D. 1995, ApJ, 454, 910